OPEN ACCESS
Journal of Innovative Optical Health Sciences
Vol. 15, No. 5 (2022) 2250031 (11 pages)

DOI: 10.1142/S1793545822500316

World Scientific
www.worldscientific.com

U-Net-based deep learning for tracking and quantitative analysis of intracellular vesicles in time-lapse microscopy images

Zhichao Liu[*,†], Heng Zhang[*], Luhong Jin[*,†], Jincheng Chen[*,†], Alexander Nedzved[‡], Sergey Ablameyko[‡], Qing Ma[§], Jiahui Yu[¶] and Yingke Xu[*,†,¶,‖,**]

[*]*Department of Biomedical Engineering*
MOE Key Laboratory of Biomedical Engineering
State Key Laboratory of Modern Optical Instrumentation
Zhejiang Provincial Key Laboratory of Cardio-Cerebral Vascular Detection Technology and Medicinal Effectiveness Appraisal
Zhejiang University, Hangzhou 310027, P. R. China

[†]*Alibaba-Zhejiang University Joint Research Center of Future Digital Healthcare, Hangzhou 310027, P. R. China*

[‡]*National Academy of Sciences*
United Institute of Informatics Problems
Belarusian State University, Minsk 220012, Republic of Belarus

[§]*Hangzhou Dowell Photonics Measurement Company Limited*
Hangzhou 310000, P. R. China

[¶]*Binjiang Institute of Zhejiang University*
Hangzhou 310053, P. R. China

[‖]*Department of Endocrinology*
Children's Hospital of Zhejiang University School of Medicine
National Clinical Research Center for Children's Health
Hangzhou, 310051 China
[**]*yingkexu@zju.edu.cn*

Received 22 January 2022
Accepted 5 June 2022
Published 29 July 2022

Fluorescence microscopy has become an essential tool for biologists, to visualize the dynamics of intracellular structures with specific labeling. Quantitatively measuring the dynamics of moving objects inside the cell is pivotal for understanding of the underlying regulatory mechanism. Protein-containing vesicles are involved in various biological processes such as material transportation,

[**]Corresponding author.

organelle interaction, and hormonal regulation, whose dynamic characteristics are significant to disease diagnosis and drug screening. Although some algorithms have been developed for vesicle tracking, most of them have limited performance when dealing with images with low resolution, poor signal-to-noise ratio (SNR) and complicated motion. Here, we proposed a novel deep learning-based method for intracellular vesicle tracking. We trained the U-Net for vesicle localization and motion classification, with demonstrates great performance in both simulated datasets and real biological samples. By combination with fan-shaped tracker (FsT) we have previously developed, this hybrid new algorithm significantly improved the performance of particle tracking with the function of subsequently automated vesicle motion classification. Furthermore, its performance was further demonstrated in analyzing with vesicle dynamics in different temperature, which achieved reasonable outcomes. Thus, we anticipate that this novel method would have vast applications in analyzing the vesicle dynamics in living cells.

Keywords: Deep learning; image processing; vesicle tracking; fluorescence microscopy; U-Net.

1. Introduction

As optics and computer science develop, advanced microscopy technologies have opened new eyesight for biomedical researchers. Fluorescence microscopy has been widely used in biomedical research to observe subcellular structures with specific labeling.[1,2] These technologies enable us to acquire quantities of time-lapse images, which contain assorted biomedical information. At the same time, we are confronted with new challenges of digesting these images by quantitatively processing the data. Due to the limitation of imaging speed, spatial resolution, and fluorescent bleach, traditional image processing methods could not perform robustly on microscopy images.[3–5]

As a method of representational learning of data,[6] deep learning has developed and evolved in many scientific fields, including microscopy image processing. Deep learning models, such as convolution neural network (CNN), recurrent neural network (RNN), generative adversarial nets (GANs), have achieved satisfactory results in many tasks, for instance image classification, object detection, image segmentation, object tracking and super-resolution reconstruction.[7,8] Multi-object tracking (MOT) is the task of following objects through a series of time-lapse images.[9,10] Measuring the velocity and dynamics of intracellular objects over time is essential to analyze the underlying biological mechanisms. For example, the trajectory of the nucleus is related to cell localization,[11,12] the dynamic information of the microtubule is associated with cell mitosis.[13,14] Intracellular vesicles have proved to be involved in many cellular processes, such as material transportation, organelle interaction, and hormonal regulation, whose dynamic characteristics are significant to disease diagnosis and drug screening.[1,15–17]

Object tracking tasks can be divided into two steps, namely object localization and data association.[18] For microscopy images, low signal-to-noise ratio (SNR) and resolution, unpredicted overlapping, and deformation are the main challenges for precise localization. Conventional data association algorithms[19,20] are always based on a specific motion model, which fails to track vesicles varying in different states of motion. In addition, the random appearance and disappearance of the moving objects further make the targets hard to follow.

U-Net is one of the most widely used models in segmentation tasks, named for its U-shaped network structure.[21] U-Net is a derivative of fully-convolution network, which can realize the translation from image to image, with its skip-connection structure accelerating training. It performs well on microscopy image segmentation tasks. Thus, in this study, we applied U-Net to intracellular vesicle localization and motion classification, which effectively improves the performance of particle tracking. We further quantified the dynamic characteristics of intracellular vesicles according to the tracking results and achieved satisfactory outcomes in cell experiments.

2. Methods

2.1. *Dataset*

2.1.1. *Cell dataset*

Cell culture and transfection

COS-7 monkey fibroblasts were cultured in high-glucose Dulbecco's modification Eagle's medium

(DMEM, Corning, Manassas, VA, USA) with 10% fetal bovine serum (FBS, Gibco, Life Technologies, USA) and 1% penicillin G/streptomycin at 37°C in a humidified 5% CO_2 incubator. According to the manufacturer's protocol, the cells were transiently transfected with transferrin receptor (TfR)-mCherry plasmid (purchased from Addgene, Catalog #55144) using Lipofectamine 3000 (Thermo Fisher).

Live-cell imaging

COS-7 fibroblasts were cultured on 35 mm glass-bottom dishes and imaged 18–24 h after transfection. Before imaging, cells were cultured in KRBH buffer, pH 7.4. Cells were kept in a thermostat-controlled chamber at 37°C throughout the imaging process. Finally, the cells were imaged in glass-bottom dishes by total internal reflection fluorescent microscope (TIRFM). The TIRFM system was based on an Nexcope NIB900 microscope, equipped with a 100× NA 1.49 oil immersion objective. The 488 nm argon laser was used to excite labeled fluorophores. Time-lapse images were taken by Andor iXon887 EMCCD under the control of iQ3 software. Representative video is provided in Supplementary Video S1.

Image preprocessing and manual annotation

The contrast and brightness of the acquired images were adjusted using ImageJ (NIH). Then the images were denoised using difference of Gaussian (DoG) filter with python program.[22,23] Finally, vesicles in the time-lapse images were annotated by biological experts and box-bounded using Colabeler AI Labeling Tool.

Data augmentation

Data augmentation refers to creating more data by transforming the original data without adding the original data. It can increase the amount and enrich the diversity of data. $256 * 256$-pixel windows are set and shifted on the fluorescence images, cropping five fields on the corners and center of each image. Then, each field is rotated clockwise by 0°, 90°, 180°, and 270°. The images are then horizontally and vertically overturned. Finally, the brightness and SNR are, respectively, adjusted. The results of data augmentation are shown in Fig. S1.

2.1.2. *Simulated dataset*

Settings and parameters

To better simulate the statistical characteristics of the vesicles, we used the distribution feature, velocity, and dynamics from the real biological data. We generated 100 simulated image sequences, and each has 50 frames. In the first frame, 30–50 vesicles were randomly distributed as diffraction-limited spots with an initial location. In the meantime, new vesicles randomly appear at each frame. The technical details are set in the following way: (1) The size of the images is $256 * 256$ pixels. (2) The motion states of vesicles were varied from directed motion, Brownian motion to restricted motion. (3) Time-lapse centroid images and trajectories were used as ground truth.

Microscope's point spread function

Because of diffraction, the image produced by the optics system is not the ideal geometric point image but a light spot (Airy spot) with a specific size, which can be defined as a point spread function (PSF).[24–26] We defined a kernel of size $5 * 5$ pixels, whose intensity decreased from the center to the edge. The kernel convolved the centroid image to convert each point as a light spot.

Microscopic noise

Noises involved in microscopic images can be divided into device-based noise and sample-based noise. The device-based noise is formed by photon scattering, electromagnetic interference, and other factors. It is random and roughly follows Poisson distribution,[23] which can be simulated by Gaussian noise using Python's Random Library. The sample-based noise comes from spontaneous fluorescence. Many background noises in real cell fluorescence images were collected and augmented, added to the synthesized images to simulate the sample-based noise. Finally, we used 80% as the training data while the remaining was used for testing. The simulation flowchart and result are shown in Fig. 1, and the representative video is provided in Supplementary Video S2.

2.2. *Proposed algorithm*

The proposed method constitutes four separate steps: (1) Localize intracellular vesicle at each frame with U-Net; (2) Classify the motion of each vesicle with U-Net; (3) Connect the centroids among successive frames by using fan-shaped tracker (FsT)[20,27] and nearest neighbor association (NNA); (4) Quantitatively quantify the dynamics of vesicle movement. The modules of the proposed method and the architecture of the proposed network are shown in Fig. 2. The proposed network consists of

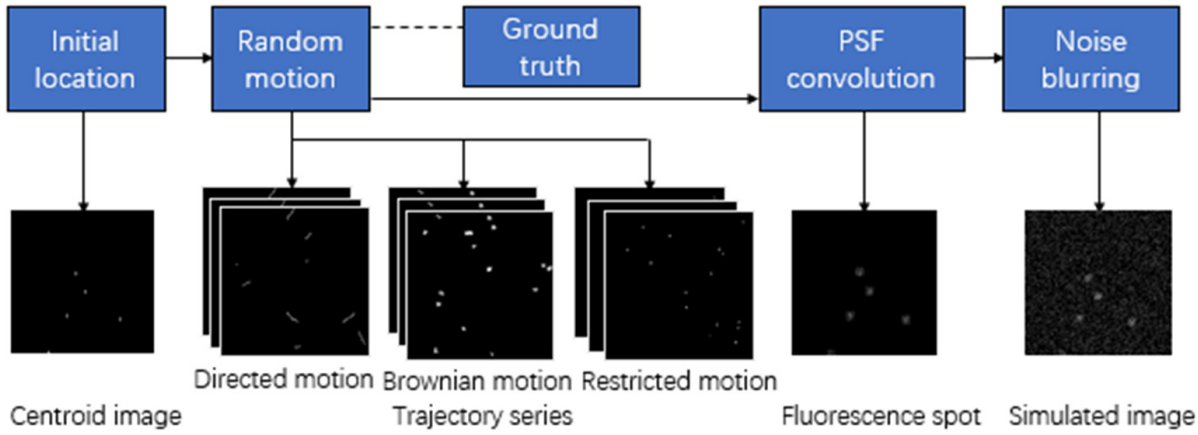

(a)

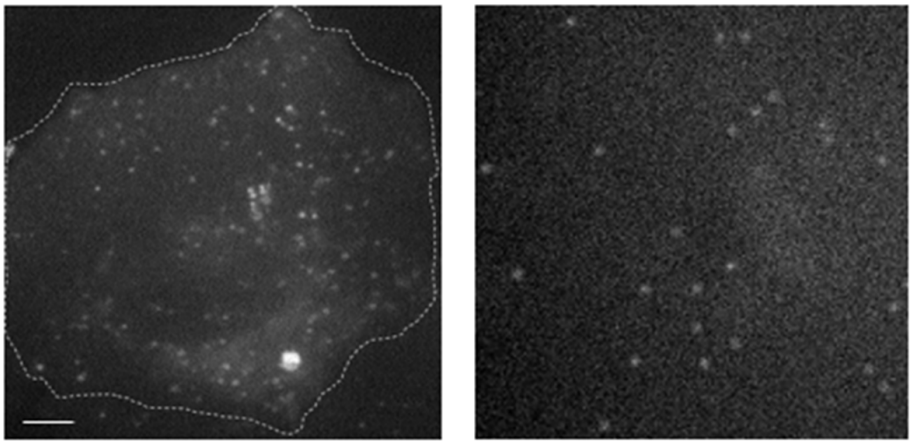

(b) (c)

Fig. 1. Simulation flowchart and representative images. (a) The simulation approach for modeling intracellular vesicle track. (b) Real fluorescence microscopy image. (c) Simulated image. Scale bar: 10 μm.

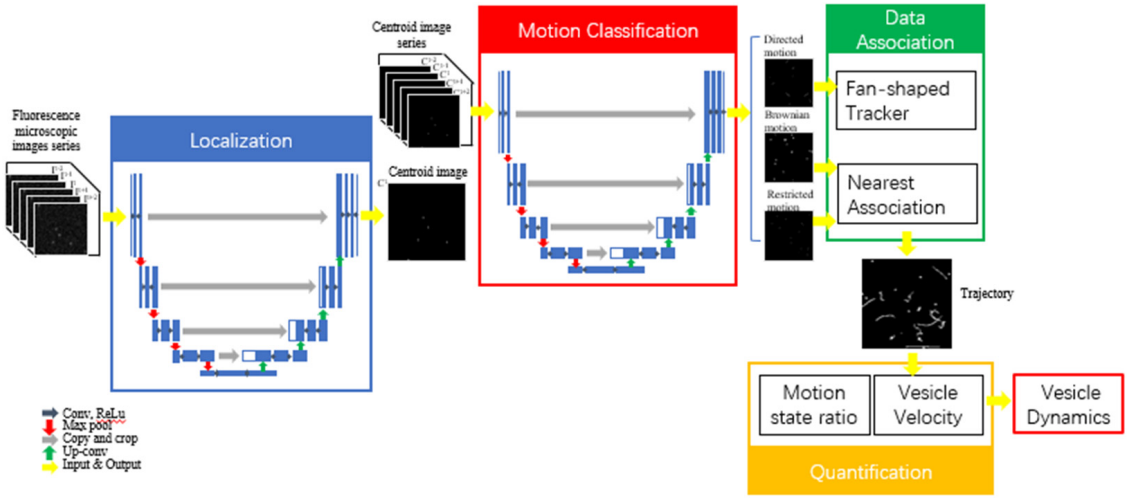

Fig. 2. Overview of the proposed method and architecture of the proposed network to extract dynamic information from fluorescence microscopy image sequences.

two U-Nets. The first one is for object localization, while the second is for motion classification. U-Net consists of two processes: down-sampling and up-sampling. The down-sampling is realized by convolution and max-pooling layers, which extracts image features and increases the size of the sensing field, ensuring the robustness of the model and decreasing the risk of overfitting. The up-sampling is achieved by deconvolution, which restores and decodes the abstract features. The skip-connection between layers is used to solve the problem of gradient explosion and attenuation as the network deepens.

2.2.1. *Localization*

During the training step, the inputs to the first U-Net were a series of fluorescence microscopy images, while the ground truth was a series of centroid images. To provide temporal information at the input, we used the frames at the neighborhood of the current frame. The loss function is defined as Eq. (1), where L represents the difference between predicted result PD and the ground truth GT, the W and H refers to the width and height of the image. We pre-trained the model on the simulated datasets, and then we retrained it by loading the pre-trained model into the real data with the method of transfer learning to obtain the final model.

$$L = \frac{1}{W \times H}\left(\sum_{i=1}^{W}\sum_{j=1}^{H} \mathrm{abs}(\mathrm{GT}(i,j) - \mathrm{PD}(i,j))\right). \tag{1}$$

2.2.2. *Data association*

As previously mentioned, conventional data association algorithms are always based on a certain motion model. However, the movement of intracellular vesicles varies, which can be categorized into three types: Brownian motion, directed motion, and restricted motion. Using the U-Net proposed previously, we classified each vesicle into a certain state of motion. The inputs were successive frames of acquired centroid images, while the ground truth were centroid images of the middle frame in three channels, respectively, corresponding to the three motion states. The loss function is defined as Eq. (2), where L represents the difference between predicted result PD and the ground truth GT, W and H refers to the image's width and height, and C_k refers to the kth channel of output.

$$L = \frac{1}{3W \times H}\left(\sum_{k=1}^{3}\sum_{i=1}^{W}\sum_{j=1}^{H} \mathrm{abs}(C_k\mathrm{GT}(i,j) - C_k\mathrm{PD}(i,j))\right) \tag{2}$$

In practical application, the data input into the model is not a completely accurate vesicle centroid map. However, it results in false negative and false positive caused by the algorithm's detection error, significantly impacting on the motion classification task. In order to improve the robustness of the model, input centroid images with 10% false-negative and 10% false-positive are used to retrain the model using transfer learning.[28] Then we, respectively, applied FsT to track vesicles of directed motion and NNA to track vesicles of Brownian motion and restricted motion.

2.2.3. *Dynamics quantification*

Vesicle dynamics definition

The movement of intracellular vesicles can be divided into Brownian motion, directed motion, and restricted motion. Different categories correspond to different physiological states and functions. With the occurrence of internal physiological reactions and the influence of external environment, the motion state of intracellular vesicles will change frequently. The proportion of each state can be used to analyze the dynamics of vesicles quantitatively. In addition, the vesicle velocity indicates the efficiency of material transportation and can be used as a quantitative index to evaluate cell dynamics. Thus, we defined the vesicle dynamics by percentage of the three different motion states and quantified vesicle velocity.

Experiment validation

Many life processes such as vesicle transportation in cells are related to temperature. The optimal temperature for endothermy cells is 37°C. If the temperature decreases, cell activity will be affected, manifested as the weakening of dynamic characteristics of subcellular structures such as vesicles.

The fluorescent cell samples transfected with TfR-mCherry plasmid were placed in the live-cell station. The fluorescent image sequences were taken at 37°C, 25°C, and 10°C water baths. The time-lapse image sequences were then analyzed with the proposed algorithm, acquiring relevant dynamic

characteristics. The video is provided in Supplementary Videos S3–S5.

3. Results and Discussion

3.1. *Localization*

Figure 3 illustrates the performance of feature particle detection (FPD)[29] and the proposed method on vesicle localization. The proposed network could localize most of the vesicles precisely in the image. Conventional values Jaccard similarity coefficient (JSC), false negative ratio (FNR), false positive ratio (FPR) are employed to quantitatively evaluate the localization performance.[30–32] The values are listed in Table 1, which shows that the proposed method surpasses the existing method on both simulated and real datasets.

In real biological dataset, the JSC on testing data is relatively lower than that on training data, which indicates that overfitting may occur. It is because our network is trained on a small dataset. Table 2 illustrates the performance of U-Net under a different source of training and testing dataset. When training and testing data comes from similar sources, the network can improve better accuracy. This informs us that a large dataset containing fluorescent images of different cells and microscope systems should be established.

Table 1. Localization performance in terms of JSC, false negative rate (FNR), and false positive rate (FPR) of proposed U-Net and FPD.

Dataset	Method	FNR↓	FPR↓	JSC↑
Simulated and training	U-Net	0.001	0.001	0.998
Real and training	U-Net	0.002	0.000	0.998
Simulated and testing	U-Net	0.037	0.027	0.939
	FPD	0.073	0.026	0.901
Real and testing	U-Net	0.140	0.116	0.744
	FPD	0.211	0.096	0.693

Table 2. Localization accuracy of U-Net under different source of training and testing datasets.

Source of training and testing data	Training JSC	Testing JSC
Different cell	0.968	0.744
Same cell and different scene	0.954	0.803
Same cell and same scene	0.956	0.946

3.2. *Data association*

The motion classification performance of U-Net with a varied number of input frames (N) was shown in Table S1. With the increase of N, the classification accuracy improves and gradually converges. As previously mentioned, detection of false negative and false positive may greatly influence vesicle motion classification. Table 3 shows the

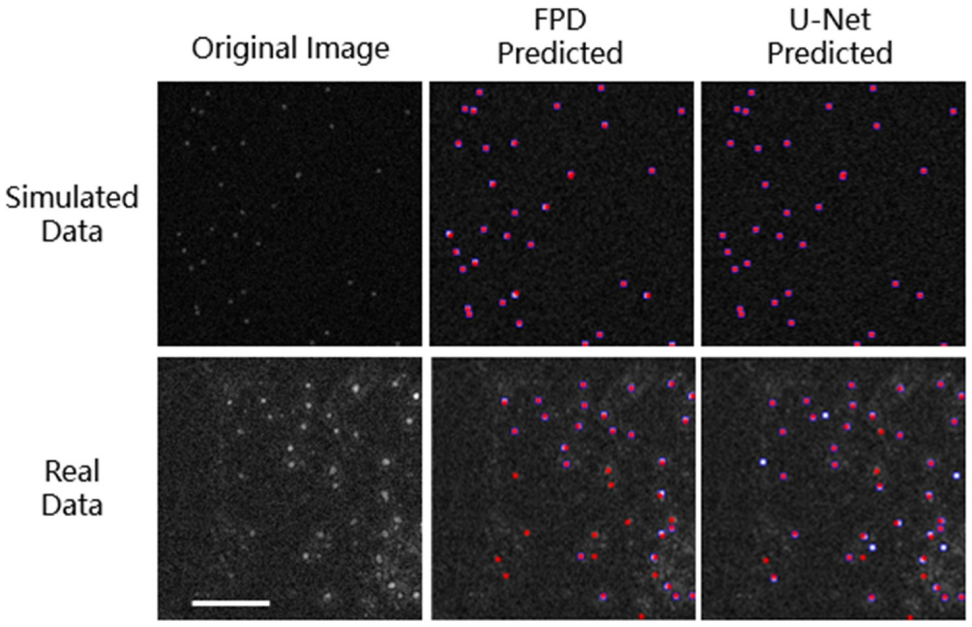

Fig. 3. Original image, FPD predicted result, and U-Net predicted vesicle localization results on simulated data and real data. The red stars stand for ground truth. In contrast, the blue boxes stand for predicted results. Scale bar: 10 μm.

Table 3. Effect of detection false negative and FPR on motion classification on original trained and retrained model (number of input frames = 7).

Input centroid image	Model	Directed motion	Brownian motion	Restricted motion	Weighted average
Ground truth	Original	0.927	0.949	0.978	0.954
10%FN, 10%FP	Original	0.521	0.795	0.835	0.747
10%FN, 10%FP	Retrained	0.851	0.852	0.850	0.851

effect of detection false negative and FPR on motion classification on original trained and retrained model. After retraining, the accuracy significantly recovers from 74.7% to 85%. Figure 4 illustrates that our proposed method has better centroid association performance than FsT. The association performance of tracking methods with or without motion classification were summarized in Table 4. GT and PD represent the ground truth and prediction of motion classification, respectively. Obviously, our proposed deep learning-based method can

Table 4. Data association algorithms' performance with/without motion classification (number of input frames = 7).

Data association algorithm	JSC	FNR	FPR
FST	0.623	0.321	0.120
FST + NNA + MC(GT)	0.991	0.006	0.003
FST + NNA + MC(PD)	0.936	0.046	0.020

significantly reduce the mismatching and improve the accuracy of centroid association. Furthermore, as shown in Fig. 5, the proposed vesicle tracking algorithm could track single vesicles and classify different vesicle motions with great accuracy.

3.3. *Dynamics quantification*

The dynamics quantification performance of the proposed method in simulated datasets was summarized in Table 5. The relative error of each index is less than 10%, which indicates that the proposed method could quantitatively analyze the dynamic characteristics of intracellular vesicles precisely. We further applied our method to quantitative analyze the vesicle dynamics under different temperatures. The results are shown in Fig. 6, which demonstrates

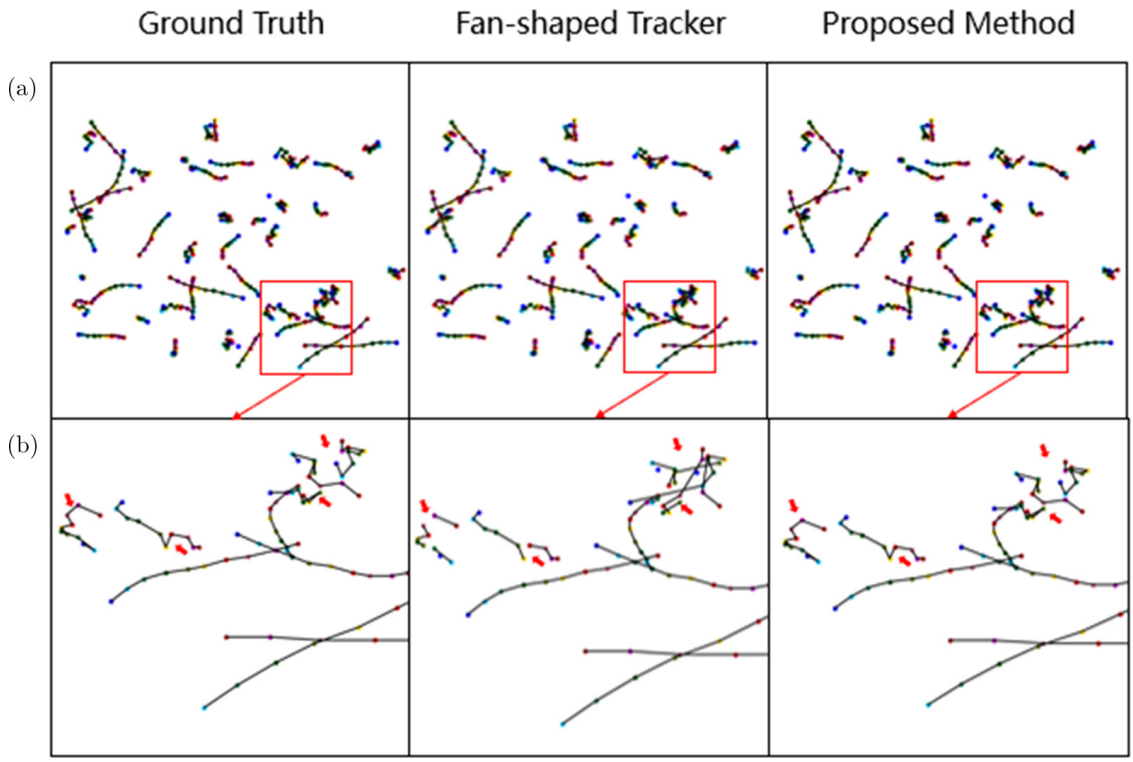

Fig. 4. Centroid association performance. (a) Ground truth and result of data association on simulated data predicted by FsT and our proposed method. (b) Enlarged views of region squared in (a), the differences of trajectories were marked with red arrows.

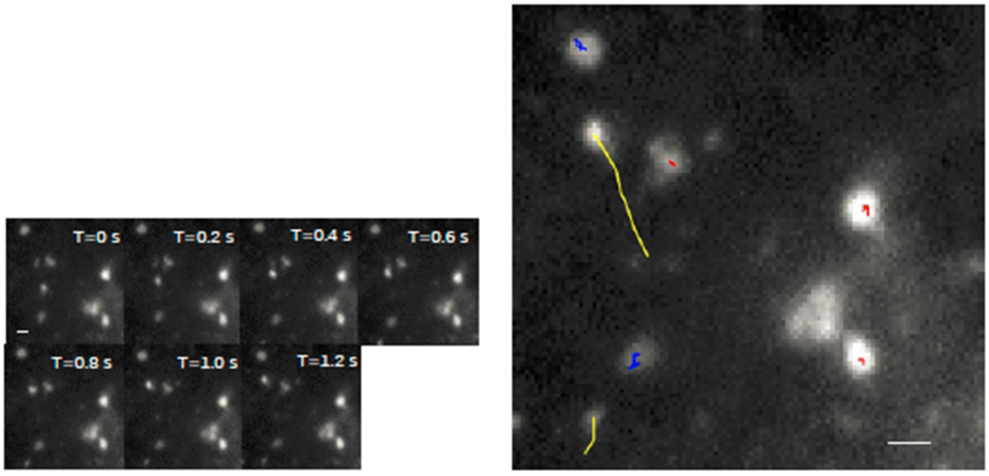

(a) (b)

Fig. 5. Application results of the proposed vesicle tracking algorithm in real vesicle image sequences. (a) Representative vesicle moving sequences (frame rate of 5 fps); (b) Motion state classification and tracking results, the yellow track represents directed motion, the blue track represents Brownian motion, and red track represents restricted motion. Scale bar = 1 μm.

Table 5. Dynamic characteristics quantification performance of our proposed method in simulation dataset.

Dynamic characteristics	Ground truth	Predicted result	Relative error
Ratio of restricted motion	0.240	0.250	0.040
	0.568	0.567	0.002
Ratio of directed motion	0.129	0.128	0.006
	0.486	0.451	0.071
Ratio of Brownian motion	0.254	0.269	0.059
	0.503	0.515	0.024
Average velocity (μm/s)	0.258	0.268	0.038
	0.313	0.311	0.007
	0.409	0.403	0.015

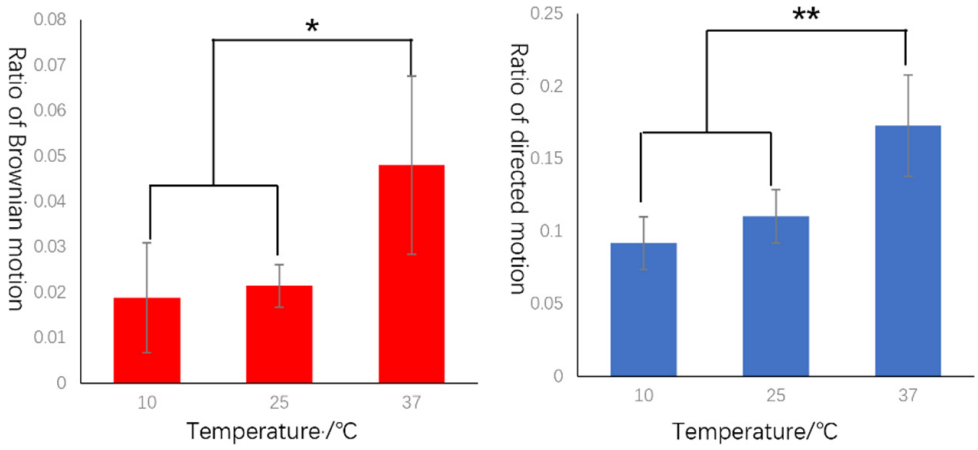

(a) (b)

Notes: * means statistically different ($p < 0.05$), ** means significantly different ($p < 0.01$), N.S means no significance ($p > 0.05$).

Fig. 6. Quantitative analysis of dynamic characteristics of vesicles at different temperatures. (a) Percentage of Brownian motion vesicles at different temperatures; (b) Percentage of directional motion vesicles at different temperatures; (c) Percentage of restricted motion vesicles at different temperatures; (d) Average percentage of directional motion vesicles at different temperatures.

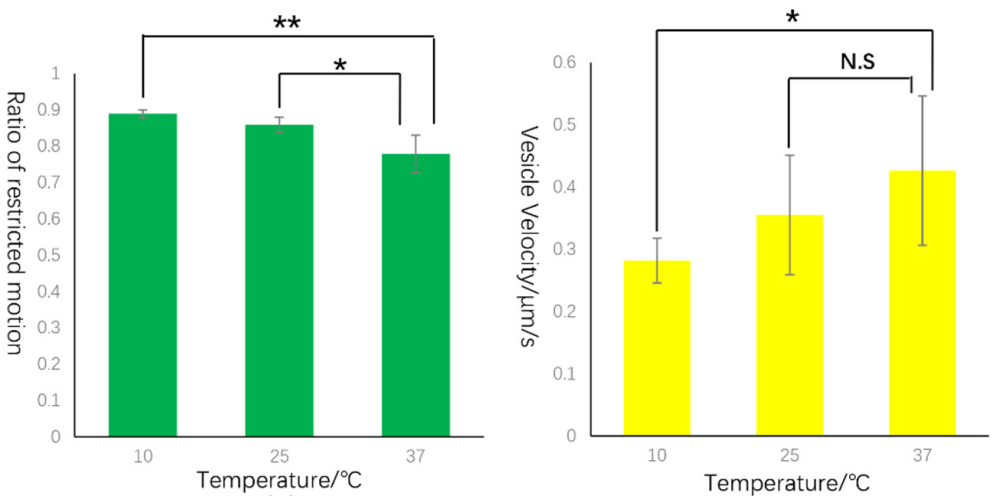

(c) (d)

Fig. 6. (*Continued*)

that the dynamics of vesicles movements, as evaluated by percentage of directed movement and the velocity of moving vesicles were correlating with elevated temperature. The concrete data are shown in Table S2. As temperature decreases, the ratio of Brownian motion and directed motion reduces, while the ratio of restricted motion improves. Moreover, the average velocity of vesicles decreases, which fits with expectations according to relevant physiological law.

4. Conclusion

In this paper, we presented a novel deep learning-based tracking method for intracellular vesicles in fluorescent microscopy image sequences. We collected real vesicle movement videos and manually annotated the vesicle trajectories. We simulated the movements of intracellular vesicles and the microscopy imaging procedure to acquire synthetic datasets. We applied U-Net, which is first proposed for segmentation of microscopy images, to perform localization and motion classification tasks and received satisfactory results. Conventional tracking algorithms are always based on a specific model of motion, for which they have limited applications on intracellular vesicles with various motion states. Although we achieved robust data association performance through combining motion classification procedures, the drawbacks of deep learning that require huge quantity of annotated and diverse datasets should not be neglected. To overcome this challenge, we tried to simulate and train our models in synthetic datasets with diverse SNR levels. By using transfer learning strategy, we believe the performance of our model could be further improved in the future.

In conclusion, this study provides biologists with tools to track intracellular vesicles. It demonstrates significant advantages in images with various motion states, which is the major challenge for traditional tracking methods. Meanwhile, the proposed method can be applied for other subcellular organelles tracking such as microtubule and mitochondria. We anticipate it will have significant applications in computer-aided diagnosis and drug screening in cells.

Conflict of Interest

The authors declare no competing interests.

Acknowledgments

This work was supported by the National Key Research and Development Program of China (2021YFF0700305 and 2018YFE0119000), the National Natural Science Foundation of China (22104129 and 62105288), Zhejiang Province Science and Technology Research Plan (2022C03014), the Fundamental Research Funds for the Central Universities (2021XZZX022) and Alibaba Cloud.

References

1. J. Wu, Y. Xu, Z. Feng, X. Zheng, "Automatically identifying fusion events between GLUT4 storage vesicles and the plasma membrane in TIRF microscopy image sequences," *Comput. Math. Methods Med.* **2015**, 610482 (2015).
2. J. G. Burchfield, J. A. Lopez, K. Mele, P. Vallotton, W. E. Hughes, "Exocytotic vesicle behaviour assessed by total internal reflection fluorescence microscopy," *Traffic* **11**(4), 429–439 (2010).
3. E. Moen, D. Bannon, T. Kudo, W. Graf, M. Covert, D. Van Valen, "Deep learning for cellular image analysis," *Nat. Methods* **16**(12), 1233–1246 (2019).
4. Z. Liu, L. Jin, J. Chen, Q. Fang, S. Ablameyko, Z. Yin, Y. Xu, "A survey on applications of deep learning in microscopy image analysis," *Comput. Biol. Med.* **134**, 104523 (2021).
5. G. Litjens, T. Kooi, B. E. Bejnordi, A. A. A. Setio, F. Ciompi, M. Ghafoorian, J. van der Laak, B. van Ginneken, C. I. Sanchez, "A survey on deep learning in medical image analysis," *Med. Image Anal.* **42**, 60–88 (2017).
6. Y. LeCun, Y. Bengio, G. Hinton, "Deep learning," *Nature* **521**(7553), 436–444 (2015).
7. E. Meijering, "A bird's-eye view of deep learning in bioimage analysis," *Comput. Struct. Biotechnol. J.* **18**, 2312–2325 (2020).
8. X. Fuyong, X. Yuanpu, S. Hai, L. Fujun, Y. Lin, "Deep learning in microscopy image analysis: A survey," *IEEE Trans. Neural Netw. Learn. Syst.* **29**(10), 4550–4568 (2018).
9. A. Bewley, Z. Ge, L. Ott, F. Ramos, B. Upcroft, Simple online and realtime tracking, *2016 IEEE International Conference on Image Processing (ICIP)* (IEEE, 2016), pp. 3464–3468.
10. G. Ciaparrone, F. Luque Sánchez, S. Tabik, L. Troiano, R. Tagliaferri, F. Herrera, "Deep learning in video multi-object tracking: A survey," *Neurocomputing* **381**, 61–88 (2020).
11. S. Cooper, A. R. Barr, R. Glen, C. Bakal, "NucliTrack: An integrated nuclei tracking application," *Bioinformatics* **33**(20), 3320–3322 (2017).
12. P. Yuan, A. Rezvan, X. Li, N. Varadarajan, H. Van Nguyen, "Phasetime: Deep learning approach to detect nuclei in time lapse phase images," *J. Clin. Med.* **8**(8), 1159 (2019).
13. A. Matov, K. Applegate, P. Kumar, C. Thoma, W. Krek, G. Danuser, T. Wittmann, "Analysis of microtubule dynamic instability using a plus-end growth marker," *Nat. Methods* **7**(9), 761–768 (2010).
14. S. Masoudi, A. Razi, C. H. G. Wright, J. C. Gatlin, U. Bagci, "Instance-level microtubule tracking," *IEEE Trans. Med. Imaging* **39**(6), 2061–2075 (2020).
15. M. Liebel, J. O. Arroyo, V. S. Beltrán, J. Osmond, A. Jo, H. Lee, R. Quidant, N. F. van Hulst, "3D tracking of extracellular vesicles by holographic fluorescence imaging," *Sci. Adv.* **6**(45), eabc2508 (2020).
16. W. Zhang, J. Gu, Y. Li, W. Shan, Y. Xu, Y. Chen, "Single-vesicle tracking reveals the potential correlation of the movement of cell-bound membrane vesicles (CBMVs) with cell migration," *Biochim. Biophys. Acta, Mol. Cell Res.* **1867**(11), 118804 (2020).
17. P. J. Kunz, L. Barthel, V. Meyer, R. King, "Vesicle transport and growth dynamics in Aspergillus niger: Microscale modeling of secretory vesicle flow and centerline extraction from confocal fluorescent data," *Biotechnol. Bioeng.* **117**(9), 2875–2886 (2020).
18. J. M. Newby, A. M. Schaefer, P. T. Lee, M. G. Forest, S. K. Lai, "Convolutional neural networks automate detection for tracking of submicron-scale particles in 2D and 3D," *Proc. Natl. Acad. Sci. USA* **115**(36), 9026–9031 (2018).
19. P. Billoir, S. Qian, "Simultaneous pattern recognition and track fitting by the Kalman filtering method," *Nucl. Instrum. Methods Phys. Res. A, Accel. Spectrom. Detect. Assoc. Equip.* **294**(1–2), 219–228 (1990).
20. L. Jin, F. Zhao, W. Lin, X. Zhou, C. Kuang, A. Nedzved, S. Ablameyko, X. Liu, Y. Xu, "Development of fan-shaped tracker for single particle tracking," *Microsc. Res. Tech.* **83**(9), 1056–1065 (2020).
21. O. Ronneberger, P. Fischer, T. Brox, U-Net: Convolutional networks for biomedical image segmentation, *Medical Image Computing and Computer-Assisted Intervention – MICCAI 2015*. PT III, (2015), pp. 234–241.
22. M. Neumann, D. Gabel, "Simple method for reduction of autofluorescence in fluorescence microscopy," *J. Histochem. Cytochem.* **50**(3), 437–439 (2002).
23. I. T. Young, "Quantitative microscopy," *IEEE Eng. Med. Biol. Mag.* **15**(1), 59–66 (1996).
24. G. B. Airy, I. On the diffraction of an annular aperture: To the editors of the philosophical magazine and journal, *Lond. Edinb. Philos. Mag. J. Sci.* **18** (114), 1–10 (1841).
25. E. Abbe, "Beiträge zur Theorie des Mikroskops und der mikroskopischen Wahrnehmung: I. Die Construction von Mikroskopen auf Grund der Theorie," *Arch. Mikr. Anat.* **9**(1), 413–418 (1873).
26. L. Rayleigh, "On the theory of optical images, with special reference to the microscope," *J. R. Microsc. Soc.* **23**(4), 474–482 (1903).
27. L. Jin, F. Zhao, W. Lin, X. Zhou, C. Kuang, L. Xu, S. Ablameyko, Y. Xu, "Fan-shaped tracker (FsT) for particle trajectory reconstruction," *Optics in Health Care and Biomedical Optics IX* **11190**, 111900Y (2019).

28. K. Weiss, T. M. Khoshgoftaar, D. Wang, "A survey of transfer learning," *J. Big Data* **3**(1), 1–40 (2016).
29. J. Wu, "Subcellular spot detection methods for fluorescences microscopic images," *Chin. J. Biomed. Eng.* **31**, 925–933 (2012).
30. M. Tang, Y. Kaymaz, B. L. Logeman, S. Eichhorn, Z. S. Liang, C. Dulac, T. B. Sackton, "Evaluating single-cell cluster stability using the Jaccard similarity index," *Bioinformatics* **37**(15), 2212–2214 (2021).
31. N. Joseph, C. Kolluru, B. A. M. Benetz, H. J. Menegay, J. H. Lass, D. L. Wilson, "Quantitative and qualitative evaluation of deep learning automatic segmentations of corneal endothelial cell images of reduced image quality obtained following cornea transplant," *J. Med. Imaging* **7**(1), 014503 (2020).
32. J. C. Caicedo *et al.*, "Evaluation of deep learning strategies for nucleus segmentation in fluorescence images," *Cytometry A* **95**(9), 952–965 (2019).